Electrocatalysis

International Edition: DOI: 10.1002/anie.201509382
German Edition: DOI: 10.1002/ange.201509382

$Co@Co_3O_4$ Encapsulated in Carbon Nanotube-Grafted Nitrogen-Doped Carbon Polyhedra as an Advanced Bifunctional Oxygen Electrode

Arshad Aijaz, Justus Masa, Christoph Rösler, Wei Xia, Philipp Weide, Alexander J. R. Botz, Roland A. Fischer, Wolfgang Schuhmann,* and Martin Muhler**

Abstract: *Efficient reversible oxygen electrodes for both the oxygen reduction reaction (ORR) and the oxygen evolution reaction (OER) are vitally important for various energy conversion devices, such as regenerative fuel cells and metal–air batteries. However, realization of such electrodes is impeded by insufficient activity and instability of electrocatalysts for both water splitting and oxygen reduction. We report highly active bifunctional electrocatalysts for oxygen electrodes comprising core–shell $Co@Co_3O_4$ nanoparticles embedded in CNT-grafted N-doped carbon-polyhedra obtained by the pyrolysis of cobalt metal–organic framework (ZIF-67) in a reductive H_2 atmosphere and subsequent controlled oxidative calcination. The catalysts afford 0.85 V reversible overvoltage in 0.1 M KOH, surpassing Pt/C, IrO_2, and RuO_2 and thus ranking them among one of the best non-precious-metal electrocatalysts for reversible oxygen electrodes.*

Electrochemical conversion between oxygen and water has attracted great attention of the scientific community because of its potential to provide next generation energy devices such as regenerative fuel cells.[1] A regenerative fuel cell produces electricity when operating in the galvanic mode and acts as water electrolyzer, producing hydrogen and oxygen to feed the fuel cell when operating in the electrolytic mode. Electrocatalytic reactions involving the oxidation and evolution of H_2 are generally efficient, and the main challenge lies in improving the efficiency of the oxygen reduction reaction (ORR) and the oxygen evolution reaction (OER). ORR and OER proceed through multielectron transfers with different reaction intermediates and mechanisms. Consequently, designing an effective bifunctional electrocatalyst for both processes is difficult.[2,3] Platinum and its alloys are well-known ORR electrocatalysts, but are poor OER electrocatalysts. In contrast, iridium and ruthenium oxide have extraordinary OER activity, but are poor ORR catalysts.[4] Also, the high cost and scarcity of these metals severely limits their wide use in energy conversion systems.

Recently, metal–organic frameworks (MOFs) have been used as self-sacrificial templates for carbon-based nanostructured porous materials.[5] MOFs are crystalline porous materials prepared by the self-assembly of metal ions and organic linkers.[6] MOF-derived carbon–metal composites often show large surface area and hierarchical pore structures, which are necessary for high-performance ORR and OER processes.[7] However, such materials mostly suffer from a low degree of graphitization and poor contact between carbon and active metal nanoparticles. As low-cost alternatives, transition-metal oxides show catalytic activity towards both ORR and OER.[2–4,8] The poor electronic conductivity of these oxides, and hence performance, can be improved by doping with electron donors or supporting them on conductive materials, such as graphitic multiwalled carbon nanotubes (CNTs).[9] In 2010, we showed that in the presence of H_2, Co nanoparticles can efficiently catalyze the production of CNTs from ethene.[10] Moreover, it is widely accepted that CNTs can grow on most transition metals provided that a sufficient partial pressure of H_2 is present.[11] Such findings inspired us to work in the direction of reductive carbonization of MOF with a more graphitic carbon yield. Herein, we report for the first time a simple, scalable, and novel method for the synthesis of core–shell spinel Co oxide nanoparticles ($Co@Co_3O_4$) encapsulated in in situ formed N-doped carbon nanotube (CNT)-grafted carbon polyhedra by reductive carbonization of *N*-containing MOF (ZIF-67), and subsequent controlled oxidative calcination (Scheme 1). A metallic Co core with semiconducting Co_3O_4 shell is expected to improve electrocatalytic activity, as the formation of a Schottky barrier between them is favorable for charge separation.[2a] Because of the intimate contact between the $Co@Co_3O_4$ and the graphitic walls, the obtained samples showed excellent performance as bifunctional electrocatalysts for both the ORR and the OER under alkaline conditions.

N-rich ZIF-67, a highly porous zeolite type Co-MOF, was deliberately chosen as precursor as it can be converted into N-

[*] Dr. A. Aijaz, Dr. W. Xia, M. Sc. P. Weide, Prof. Dr. M. Muhler
Laboratory of Industrial Chemistry, Ruhr-University Bochum
44780 Bochum (Germany)
E-mail: muhler@techem.rub.de
Prof. Dr. M. Muhler
Max Planck Institute for Chemical Energy Conversion
45470 Mülheim an der Ruhr (Germany)
Dr. J. Masa, M. Sc. A. J. R. Botz, Prof. Dr. W. Schuhmann
Analytical Chemistry—Center for Electrochemical Sciences (CES), Ruhr-University Bochum
44780 Bochum (Germany)
E-mail: wolfgang.schuhmann@rub.de
M. Sc. C. Rösler, Prof. Dr. R. A. Fischer
Inorganic Chemistry II—Organometallics & Materials, Department of Chemistry and Biochemistry, Ruhr-University Bochum
44780 Bochum (Germany)
E-mail: roland.fischer@rub.de

Supporting information for this article can be found under http://dx.doi.org/10.1002/anie.201509382.

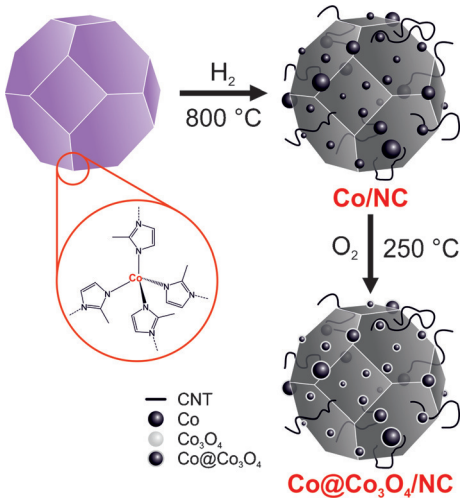

Scheme 1. Representation of the formation of core–shell $Co@Co_3O_4$ nanoparticles encapsulated in CNT-grafted N-doped carbon polyhedra by use of reductive carbonization of a N-containing MOF (ZIF-67).

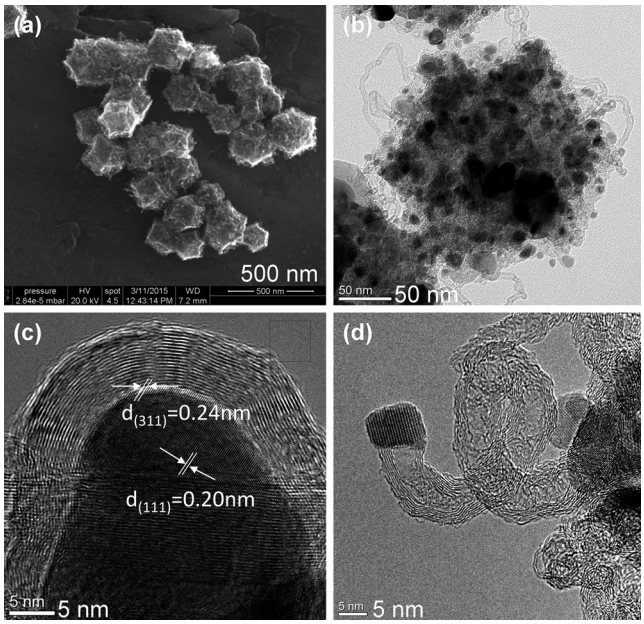

Figure 1. a) SEM and b) TEM images of Co/NC; high resolution TEM images of $Co@Co_3O_4$/NC-1 showing c) $Co@Co_3O_4$ nanoparticles embedded in graphitic layers and d) wrapped CNT.

doped carbon and Co nanoparticles. Polyhedral nanocrystals of ZIF-67 with average sizes of 200–300 nm were synthesized by slight modification of a reported procedure.[12] The synthesis of $Co@Co_3O_4$ embedded in N-doped CNT-grafted carbon polyhedra involved two steps. In the first step, ZIF-67 was directly carbonized at 800 °C for 2 h in a temperature-programmed furnace under a flow of H_2/He. The resulting material is denoted as Co/NC. This step was followed by mild calcination of the product in O_2 flow at 250 °C for 2 h. The resulting catalyst is hereafter denoted as $Co@Co_3O_4$/NC-1. Similarly, a catalyst prepared in flowing O_2 at 250 °C for 6 h is labeled $Co@Co_3O_4$/NC-2.[12] During the carbonization process, the ZIF-67 structure degrades to form N-doped porous carbons and metallic Co nanoparticles. Subsequently, the metallic Co surfaces were partially oxidized generating core–shell $Co@Co_3O_4$ nanoparticles. The embedded Co-N_x moieties and N-functionalized groups in the carbon framework, particularly, pyridinic and pyrrolic, act as complementary ORR catalysts. Furthermore, metallic Co and CNT provide high conductivity to the $Co@Co_3O_4$ nanoparticles, thereby furnishing the catalyst to catalyze both ORR and OER efficiently.

The scanning electron microscopy (SEM) image of Co/NC indicates polyhedral morphology (Figure 1 a) similar to the original single polyhedral crystals of ZIF-67 (Supporting Information, Figure S1). Transmission electron microscopy (TEM) of a single Co/NC dodecahedron revealed that it has a porous structure, in which Co nanoparticles with the size of a few nanometers (black dots) are homogenously embedded in the carbon framework (gray matrix; Figure 1 b). Interestingly, few CNTs with the lengths of 100–200 nm and diameters of 7–8 nm were seen that are wrapping the polyhedra. The spot- and ring-like patterns in the selected-area electron diffraction (SAED) image show that the Co/NC particles are polycrystalline (Supporting Information, Figure S2). The sample calcined in O_2 ($Co@Co_3O_4$/NC-1) has similar polyhedral morphology as Co/NC confirmed by SEM measurements (Supporting Information, Figure S3). High-resolution transmission electron microscopy (HRTEM) studies of $Co@Co_3O_4$/NC-1 revealed crystalline $Co@Co_3O_4$ nanoparticles wrapped with highly graphitic carbon composed of few graphene layers (Figure 1 c). The lattice fringe of the inner core of $Co@Co_3O_4$ is consistent with the Co crystal structure having {111} lattice fringes with an interspacing of 0.204 nm, and the layers outside the Co core having {311} lattice fringes with an interspacing of 0.24 nm are found to be cubic Co_3O_4.[13a,7d] There were also few graphitic CNTs having $Co@Co_3O_4$ nanoparticles residing at the tip of the CNTs (Figure 1 d). The formation of such long CNT-grafted polyhedra is a very rare example which makes such carbon materials more graphitic, and hence useful for energy conversion applications. For comparison, a sample synthesized by the conventional carbonization method using N_2 as inert atmosphere led to CNT-free polyhedra as expected (Supporting Information, Figure S4). Additionally, the high-resolution TEM image revealed a much lower degree of graphitization in comparison to $Co@Co_3O_4$/NC-1 (Supporting Information, Figure S5).

X-ray diffraction (XRD) analyses of Co/NC showed a broad peak with maxima at 26.1° originating from the (002) planes of graphitic carbon and CNTs (Figure 2 a).[13a] The peaks appearing at 44.3 and 51.7 were indexed to the (111) and (200) reflections of face-centered (fcc) Co.[13a] Extra peaks appeared in the XRD pattern of $Co@Co_3O_4$/NC-1 assigned to the cubic Co_3O_4 spinel phase.[13a] The sample $Co@Co_3O_4$/NC-2, which was treated longer with O_2, showed more intense Co_3O_4 peaks with lower intensity of metallic Co peaks. Interestingly, the graphitic peak at 26.1° became more intense because of the removal of amorphous carbon during the O_2 treatment. Such sharp graphitic peaks at 26.1° have not been observed previously in MOF-derived carbon materials. Raman spectroscopy revealed the two characteristic bands of

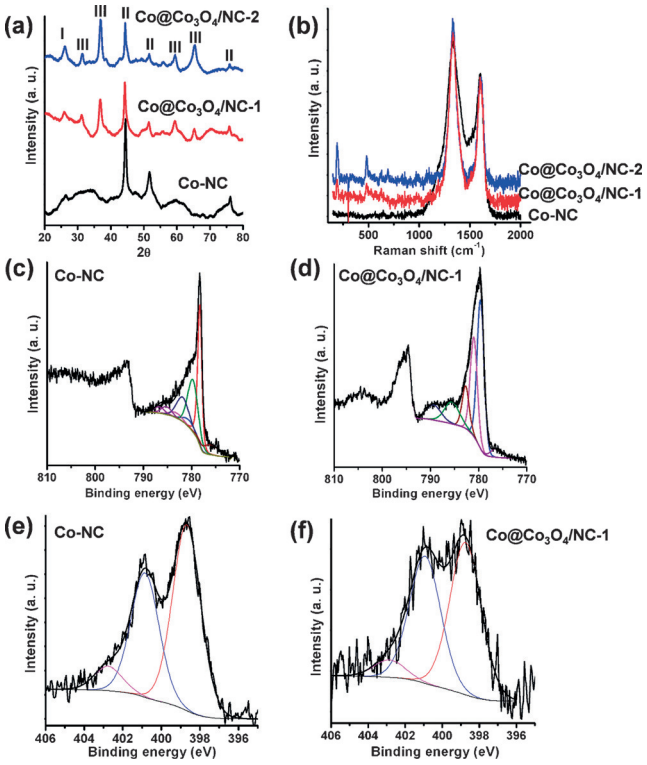

Figure 2. a) XRD patterns, the peaks labelled I, II, and III originate from graphite, metallic Co, and Co_3O_4, respectively; b) Raman spectra recorded at 661 nm laser excitation; XPS data showing c) Co 2p spectrum of Co/NC, d) Co 2p spectrum of Co@Co_3O_4/NC-1, e) N 1s spectrum of Co/NC, and f) N 1s spectrum of Co@Co_3O_4/NC-1.

graphite at 1350 cm^{-1} (D-band) and 1580 cm^{-1} (G-band) in all samples (Figure 2b). Co@Co_3O_4/NC-1, Co@Co_3O_4/NC-2 showed additional bands at nearly 193 (F_{2g}) and 480 (E_g) cm^{-1} corresponding to the spinel Co_3O_4 structure.[13b] These XRD and Raman studies suggest that Co@Co_3O_4/NC-1 and Co@Co_3O_4/NC-2 have more graphitic carbon than Co/NC, that is, during the O_2 treatment some amorphous carbon was burnt off. Also, the width of the shell (Co_3O_4) can be tuned by controlled O_2 treatment. N_2 physisorption experiments were performed at 77 K to examine the specific surface area of these materials (Supporting Information, Figure S6). The Brunauer–Emmett–Teller (BET) surface area of Co/C, Co@Co_3O_4/NC-1, and Co@Co_3O_4/NC-2 were found to be 233, 111, and 76 $m^2 g^{-1}$, respectively.

X-ray photoelectron spectroscopy (XPS) of these samples revealed the presence of C, N, O, and Co (Supporting Information, Figure S7). The C 1s peak centered at 285.5 eV is the typical graphitic carbon peak. The stronger O 1s peak at 529.8 eV in Co@Co_3O_4/NC-1 confirmed the formation of metal oxide (Supporting Information, Figure S7). A sharp metallic Co $2p_{3/2}$ peak of Co/NC appeared at 778.3 eV, while Co@Co_3O_4/NC-1 showed a Co $2p_{3/2}$ peak at 780.1 eV typical of Co_3O_4 in good agreement with well-characterized Co_3O_4 (Figure 2c,d).[7d] Deconvolution of the N 1s peak of Co/NC and Co@Co_3O_4/NC-1 resulted in a combination of pyridinic, pyrrolic, and quaternary nitrogen species with maxima located at 398.6 and 400.9 eV (Figure 2e,f). The surface N content derived from the XPS measurements in Co/NC and Co@Co_3O_4/NC-1 was 3.3 and 1.26 at%, respectively. The Co content in Co/C, Co@Co_3O_4/NC-1 and Co@Co_3O_4/NC-2 was determined by inductively coupled plasma optical emission spectroscopy (ICP-OES) and found to be 31.7, 43.1, and 40.8 wt%, respectively. These results demonstrate the formation of core–shell Co@Co_3O_4 nanoparticles embedded in CNT-wrapped polyhedra.

The electrocatalytic activities of the as-synthesized catalysts were investigated in O_2-saturated KOH (0.1M) with a catalyst loading of 210 $\mu g\,cm^{-2}$ and compared with commercial state-of-art electrocatalysts Pt/C, IrO_2, RuO_2.[12] Co/NC and Co@Co_3O_4/NC-1 showed very similar ORR activity, as indicated by the linear sweep voltammograms (LSVs) in Figure 3a, while Co@Co_3O_4/NC-2 was less active with 0.06 V

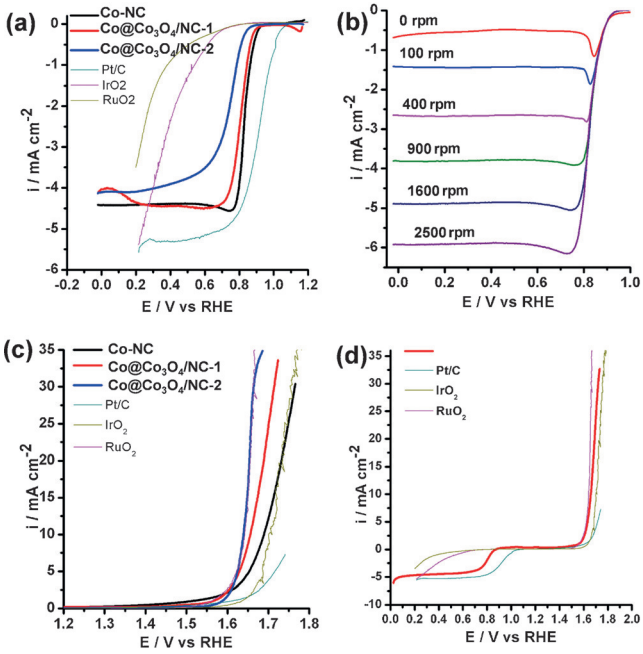

Figure 3. LSV of different electrocatalysts at 1600 rpm showing RDE electrocatalysis of a) oxygen reduction and c) water oxidation; b) LSV of Co/NC at various rotating speeds and d) a comparison of ORR and OER bifunctional activities of Co@Co_3O_4/NC-1, Pt/C, IrO_2, RuO_2. All the voltammograms were recorded in O_2-saturated 0.1 M KOH at a scan rate of 5 $mV s^{-1}$.

more anodic overpotential in comparison to Co@Co_3O_4/NC-1 at a current density of 1 $mA\,cm^{-2}$. On the other hand, Co@Co_3O_4/NC-2 showed the highest activity for oxygen-evolution having a current density of 10 $mA\,cm^{-2}$ at 1.64 V, little better than RuO_2 (Figure 3c). As a bifunctional catalyst for both ORR and OER, rotating disk electrode (RDE) voltammetry was performed and revealed that Co@Co_3O_4/NC-1 is the best catalyst in terms of bifunctional activity, that is, better OER catalyst than Pt/C, IrO_2 and very similar activity to the benchmark OER catalyst (RuO_2), and of comparable activity to the benchmark ORR catalyst (Pt/C).

The overvoltage between ORR and OER translates into loss in efficiency and is therefore an important parameter for

Table 1: The bifunctional activity of different catalysts for ORR and OER.

Catalyst	E_{ORR}/V half-wave potential	E_{OER}/V 10 mA cm^{-2}	ΔE/V ($E_{ORR}-E_{OER}$)
Co/NC	0.83	1.69	0.86
Co@Co_3O_4/NC-1	0.80	1.65	0.85
Co@Co_3O_4/NC-2	0.74	1.64	0.90
RuO_2	0.37	1.64	1.27
IrO_2	0.29	1.70	1.41
Pt/C	0.90	1.90	1.0

evaluating the bifunctional electrocatalytic activity of a given catalyst (Table 1). The ORR activities of the catalysts were derived at a potential corresponding to half of the current density during oxygen reduction, while the OER activities were calculated as the potential at a current density of 10 mA cm^{-2}, which has been proposed as Jaramillo's figure-of-merit for the bifunctional activity of a given catalyst.[4c] Strikingly, the low overvoltage between ORR and OER would translate into energy saving of at least 150 mV and 100 mV, respectively, if instead of Pt/C, the Co@Co_3O_4/NC-1 and Co@Co_3O_4/NC-2 bifunctional electrocatalysts are used.

The catalytic pathway for the ORR on as-synthesized catalysts was investigated by Koutecky–Levich (KL) plots obtained from the LSVs at various rotating speeds. Figure 3b and the Supporting Information, Figure S6 show increasing cathodic current with increasing rotating speed because of the improved mass transport at the electrode surface. From the slopes of the KL plots, the number of electrons transferred per O_2 molecule in the ORR was calculated to be 3.72 at 0.75 V (vs. RHE) for Co/NC and 3.78 for Co@Co_3O_4/NC-1, suggesting a predominantly four-electron reduction pathway to produce water as the main product (Supporting Information, Figures S9 and S10). In the KL plot (Supporting Information, Figure S10), all lines have a similar slope to the theoretical $n=4$ lines suggesting that Co@Co_3O_4/NC-1 reduces O_2 to water mostly via the four-electron transfer pathway. Tafel plots for the OER are shown in the Supporting Information, Figure S11. The Tafel slopes of Co/NC, Co@Co_3O_4/NC-1 and Co@Co_3O_4/NC-2 in the potential range between 1.6 V and 1.7 V were 125.3, 91.5, and 54.3 mV dec^{-1}, respectively. However, RuO_2, IrO_2, and Pt/C have 89.6, 86.2, and 354.9 mV dec^{-1} in the same potential window. The Tafel slope of Co@Co_3O_4/NC-2 was lower than that of Co@Co_3O_4/NC-1, indicating that the reaction was kinetically faster on the former in the potential range between 1.6 V and 1.7 V. The exact onset potential of the OER, to distinguish between water oxidation and metal oxidation, was determined using scanning electrochemical microscopy (SECM) by in situ detection of evolved O_2. An increase in the cathodic current measured at the tip commenced at about 1.56 V vs. RHE representing an overpotential of only 0.33 V for Co@Co_3O_4/NC-1 from the theoretical value of 1.23 V (Supporting Information, Figure S12). On the other hand, the onset potential for the OER on Co/C and Co@Co_3O_4/NC-2 was observed at 1.58 and 1.62 V vs. RHE, respectively (Supporting Information, Figure S13 and S14). The SECM studies revealed Co@Co_3O_4/NC-1 is the best OER catalyst with the lowest onset potential. Chronoamperometric (for ORR at 0.77 V) and chronopotentiometric (for OER at 10 mA cm^{-2}) measurements showed no significant loss in activity after 25 h and 45 h, respectively, indicating that Co@Co_3O_4/NC-1 is able to sustain a stable performance over a long period of time (Supporting Information, Figures S15 and S16).

Compared with our catalyst Co@Co_3O_4/NC-1, the catalyst synthesized conventionally using N_2 as carbonization atmosphere, denoted as Co@Co_3O_4/NC-1(N_2), showed lower activities for both ORR and OER (Supporting Information, Figure S17). Interestingly, it seems that Co@Co_3O_4/NC-1 is more stable and reduces O_2 more predominately via the 4 e$^-$ oxygen reduction pathway in comparison to previously reported catalysts synthesized by conventional carbonization methods.[14] More importantly, Co@Co_3O_4/NC-1 showed stable performance even in concentrated KOH (1.0 M) solution (Supporting Information, Figure S16). However, ZIF-derived carbons have not been much elaborated for the OER, as their performances are not as good as in the ORR.

As stated above, the MOF carbonization in H_2 can lead to more graphitic CNT-carbon composites. It is generally accepted that transition-metal nanoparticles work as catalysts for the growth of graphitic CNTs provided that a sufficient partial pressure of H_2 is present.[10,11] Herein, ZIF-67 worked as source of Co nanoparticles, carbon polyhedra and CNTs. Initially, ZIF-67 is decomposed into carbon/Co polyhedra and then Co nanoparticles worked as catalyst for the growth of graphitic CNTs in the presence of H_2. Other than CNT growth, the role of H_2 is also to clean the catalyst from the deposition of amorphous carbon. Furthermore, these CNT-grafted polyhedra can directly be grown on nickel foam. It is well-known that a high electroactive support area can enhance the electrocatalytic performance.[9] Depositing ZIF-67 solvothermally on nickel foam and subsequent carbonization in H_2 at 800 °C led to a three-dimensional (3D) electrode (Supporting Information, Figure S18). This 3D electrode is able to show very long OER durability with 1.62 V overpotential in 0.1 M KOH at 10 mA cm^{-2} current density (Supporting Information, Figure S19).

The efficiency of these catalysts, especially Co@Co_3O_4/NC-1, can be explained by 1) the highly graphitic nature of CNT-grafted polyhedra, 2) the presence of nitrogen-containing functional groups in the carbon framework, 3) the porous nitrogen-rich carbon shell surrounding the metal nanoparticles, and most importantly 4) the existence of synergy between conductive metallic Co cores and semiconductive Co_3O_4 shells. All of these characteristics confer enhanced conductivity to the particles thus concertedly promoting their activity as bifunctional catalyst especially for the OER. Also, the presence of Co-N_x or Co_3O_4-N_x units present in the samples cannot be ignored as these are considered as active sites for the ORR.[3b] However, the decrease in the ORR activities of Co@Co_3O_4/NC-1 and Co@Co_3O_4/NC-2 may be associated with a relatively lower amount of N in these samples. It would be interesting to design such core–shell metal nanoparticles with retention of a high quantity of N functionalities. Furthermore, using a MOF as sacrificial precursor is advantageous for obtaining such nanostructured polyhedra having large surface area and high dispersion of

metal/metal oxide nanoparticles. These results conclusively demonstrate the huge potential of reductive carbonization of a MOF for the synthesis of excellent bifunctional catalysts for oxygen electrodes.

In summary, a simple, easily scalable, and novel method for the synthesis of core–shell $Co@Co_3O_4$ nanoparticles embedded in in situ formed highly graphitic nitrogen-doped CNT-grafted carbon polyhedra has been developed. Using H_2 for reductive carbonization of MOF is a versatile method for grafting porous carbons with highly graphitic CNTs. These catalysts showed lower overvoltage between the ORR and OER compared to the state-of-art electrocatalysts Pt/C, IrO_2, and RuO_2. With the great variability of MOF compositions, pore structures, and coordination space for loading with dopants, this work shows the potential to design advanced oxide nanocomposite bifunctional catalysts as a replacement of expensive metals for reversible electrochemical energy storage and conversion technologies, such as metal–air batteries and regenerative fuel cells.

Acknowledgements

Financial support from the DFG (Deutsche Forschungsgemeinschaft) in the framework of the Cluster of Excellence RESOLV (EXC1069) is gratefully acknowledged.

Keywords: heterogeneous catalysts · metal nanoparticles · nanostructured materials · oxygen reduction · water oxidation

How to cite: *Angew. Chem. Int. Ed.* **2016**, *55*, 4087–4091
Angew. Chem. **2016**, *128*, 4155–4160

[1] G. Chen, S. R. Bare, T. E. Mallouk, *J. Electrochem. Soc.* **2002**, *149*, A1092.

[2] a) X. Liu, M. Park, M. G. Kim, S. Gupta, G. Wu, J. Cho, *Angew. Chem. Int. Ed.* **2015**, *54*, 9654; *Angew. Chem.* **2015**, *127*, 9790; b) A. Zhao, J. Masa, W. Xia, A. Maljusch, M.-G. Willinger, G. Clavel, K. Xie, R. Schlögl, W. Schuhmann, M. Muhler, *J. Am. Chem. Soc.* **2014**, *136*, 7551.

[3] a) M. Ledendecker, G. Clavel, M. Antonietti, M. Shalom, *Adv. Funct. Mater.* **2015**, *25*, 393; b) J. Masa, W. Xia, I. Sinev, A. Zhao, Z. Sun, S. Grützke, P. Weide, M. Muhler, W. Schuhmann, *Angew. Chem. Int. Ed.* **2014**, *53*, 8508; *Angew. Chem.* **2014**, *126*, 8648.

[4] a) D. Wang, H. L. Xin, R. Hovden, H. Wang, Y. Yu, D. A. Muller, F. J. DiSalvo, H. D. Abruña, *Nat. Mater.* **2013**, *12*, 81; b) I. Katsounaros, S. Cherevko, A. R. Zeradjanin, K. J. J. Mayrhofer, *Angew. Chem. Int. Ed.* **2014**, *53*, 102; *Angew. Chem.* **2014**, *126*, 104; c) Y. Gorlin, T. F. Jaramillo, *J. Am. Chem. Soc.* **2010**, *132*, 13612.

[5] a) H. B. Wu, B. Y. Xia, L. Yu, X.-Y. Yu, X. W. Lou, *Nat. Commun.* **2015**, DOI: 10.1038/ncomms7512; b) Y.-Z. Chen, C. Wang, Z.-Y. Wu, Y. Xiong, Q. Xu, S.-H. Yu, H.-L. Jiang, *Adv. Mater.* **2015**, *27*, 5010; c) S. Lim, K. Suh, Y. Kim, M. Yoon, H. Park, D. N. Dybtsev, K. Kim, *Chem. Commun.* **2012**, *48*, 7447; d) W. Chaikittisilp, M. Hu, H. Wang, H.-S. Huang, T. Fujita, K. C.-W. Wu, L.-C. Chen, Y. Yamauchi, K. Ariga, *Chem. Commun.* **2012**, *48*, 7259; e) B. Liu, H. Shioyama, T. Akita, Q. Xu, *J. Am. Chem. Soc.* **2008**, *130*, 5390.

[6] a) H. C. Zhou, J. R. Long, O. M. Yaghi, *Chem. Rev.* **2012**, *112*, 673; b) N. Stock, S. Biswas, *Chem. Rev.* **2012**, *112*, 933; c) S. Sen, N. N. Nair, T. Yamada, H. Kitagawa, P. K. Bharadwaj, *J. Am. Chem. Soc.* **2012**, *134*, 19432; d) S. T. Meek, J. A. Greathouse, M. D. Allendorf, *Adv. Mater.* **2011**, *23*, 249; e) A. Corma, H. Garcia, F. X. L. I. Xamena, *Chem. Rev.* **2010**, *110*, 4606; f) B. Chen, S. Xiang, G. Qian, *Acc. Chem. Res.* **2010**, *43*, 1115; g) O. K. Farha, J. T. Hupp, *Acc. Chem. Res.* **2010**, *43*, 1166; h) G. Férey, *Chem. Soc. Rev.* **2008**, *37*, 191; i) S. Kitagawa, R. Kitaura, S. Noro, *Angew. Chem. Int. Ed.* **2004**, *43*, 2334; *Angew. Chem.* **2004**, *116*, 2388.

[7] a) W. Xia, R. Zou, L. An, D. Xia, S. Guo, *Energy Environ. Sci.* **2015**, *8*, 568; b) A. Aijaz, N. Fujiwara, Q. Xu, *J. Am. Chem. Soc.* **2014**, *136*, 6790; c) W. Chaikittisilp, N. L. Torad, C. Li, M. Imura, N. Suzuki, S. Ishihara, K. Ariga, Y. Yamauchi, *Chem. Eur. J.* **2014**, *20*, 4217; d) T. Y. Ma, S. Dai, M. Jaroniec, S. Z. Qiao, *J. Am. Chem. Soc.* **2014**, *136*, 13925.

[8] a) J. Masa, W. Xia, M. Muhler, W. Schuhmann, *Angew. Chem. Int. Ed.* **2015**, *54*, 10102; *Angew. Chem.* **2015**, *127*, 10240; b) D. Gu, W. Li, F. Wang, H. Bongard, B. Spliethoff, W. Schmidt, C. Weidenthaler, Y. Xia, D. Zhao, F. Schüth, *Angew. Chem. Int. Ed.* **2015**, *54*, 7060; *Angew. Chem.* **2015**, *127*, 7166; c) F. Cheng, J. Shen, B. Peng, Y. Pan, Z. Tao, J. Chen, *Nat. Chem.* **2011**, *3*, 79.

[9] Y. Liang, Y. Li, H. Wang, J. Zhou, J. Wang, T. Regier, H. Dai, *Nat. Mater.* **2011**, *10*, 780.

[10] J. Tessonnier, M. Becker, W. Xia, F. Girgsdies, R. Blume, L. Yao, D. Su, M. Muhler, R. Schlögl, *ChemCatChem* **2010**, *2*, 1559.

[11] E. S. Aydil, M. J. Behr, E. A. Gaulding, K. A. Mkhoyan, *J. Appl. Phys.* **2010**, *108*, 053303.

[12] See the supporting information for details.

[13] a) H. Jin, J. Wang, D. Su, Z. Wei, Z. Pang, Y. Wang, *J. Am. Chem. Soc.* **2015**, *137*, 2688; b) V. G. Hadjievl, M. N. Ilievl, I. V. Vergilov, *J. Phys. C* **1988**, *21*, L199.

[14] W. Xia, J. Zhu, W. Guo, L. An, D. Xia, R. Zou, *J. Mater. Chem. A* **2014**, *2*, 11606.

Received: October 7, 2015
Revised: January 4, 2016
Published online: February 23, 2016

